Topological origin of quasi-flat edge band in phosphorene

2014 New J. Phys. 16 115004

(http://iopscience.iop.org/1367-2630/16/11/115004)

New Journal of Physics
The open access journal at the forefront of physics
Deutsche Physikalische Gesellschaft DPG | IOP Institute of Physics

Topological origin of quasi-flat edge band in phosphorene

Motohiko Ezawa
Department of Applied Physics, University of Tokyo, Hongo 7-3-1, 113-8656, Japan
E-mail: ezawa@ap.t.u-tokyo.ac.jp

Received 4 July 2014
Accepted for publication 24 September 2014
Published 31 October 2014
New Journal of Physics **16** (2014) 115004
doi:10.1088/1367-2630/16/11/115004

Abstract
Phosphorene, a honeycomb structure of black phosphorus, was isolated recently. The band structure is highly anisotropic, where the k_x direction is Dirac-like and the k_y direction is Schrödinger-like. A prominent feature is the presence of a quasi-flat edge band entirely detached from the bulk band in phosphorene nanoribbons. We explore the mechanism of the emergence of the quasi-flat band by employing the topological argument invented to explain successfully the flat band familiar in graphene. The quasi-flat band can be controlled by applying in-plane electric field perpendicular to the ribbon direction. The conductance is switched off above a critical electric field, which acts as a field-effect transistor.

Keywords: topological insulator, bulk-edge correspondence, topology, phosphorene, black phosphorus

1. Introduction

Graphene is one of the most fascinating materials found in this decade [1, 2]. The low-energy theory is described by massless Dirac fermions, which leads to various remarkable electrical properties. In practical applications to current semiconductor technology, however, we need a finite band gap in which electrons cannot exist freely. For instance, armchair graphene nanoribbons have a finite gap depending on their width [3–5], while bilayer graphene under a perpendicular electric field also has a gap [6]. It is desirable to find an atomic monolayer bulk

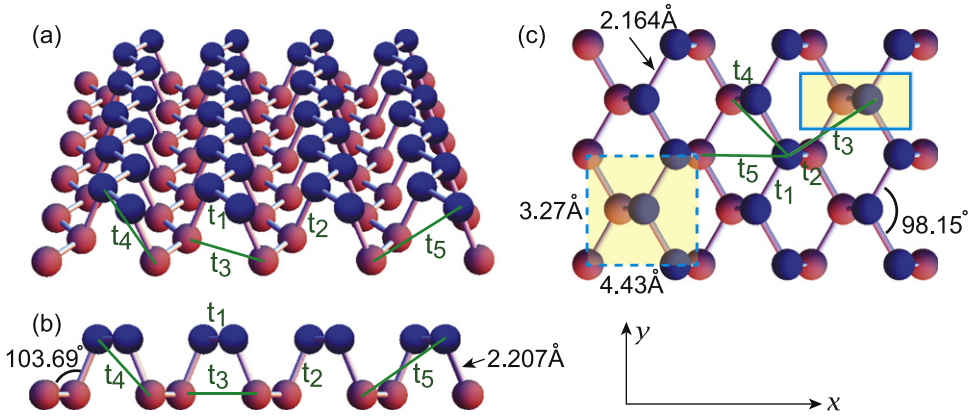

Figure 1. Illustration of the structure and the transfer energy t_i of phosphorene. (a) Bird eye's view. (b) Side view. (c) Top view. The left edge is zigzag while the right edge is beard as a nanoribbon. Red (blue) balls represent phosphorus atoms in the upper (lower) layer. A dotted (solid) rectangular denote the unit cell of the four-band (two-band) model. The parameters of the unit cell length and angles of bonds are taken from [17].

sample that has a finite gap. Silicene is a promising candidate for post graphene materials, which is predicted to be a quantum spin-Hall insulator [7]. Nevertheless, silicene has so far been synthesized only on metallic surfaces [8–10]. Another promising candidate is a transition metal dichalcogenides such as molybdenite [11–13].

A newcomer challenges the race of the post-graphene materials. That is phosphorene, a honeycomb structure of black phosphorus. It has been successfully generated in the laboratory [14–18] and has revealed a great potential in applications to electronics. Black phosphorus is a layered material where individual atomic layers are stacked together by Van der Waals interactions. Just as graphene can be isolated by peeling graphite, phosphorene can be similarly isolated from black phosphorus by the mechanical exfoliation method. As a key structure it is not planer but puckered due to the sp^3 hybridization, as shown in figure 1. There are already several works based on first-principle calculations on phosphorene [19–22] and its nanoribbon [23–27]. The edge states detouched from the bulk band have been found in pristine zigzag phosphorene nanoribbons [24–27]. The tight-binding model was proposed [28] very recently by including the transfer energy t_i over the five neighbor hopping sites ($i = 1, 2, \cdots, 5$), as illustrated in figure 1.

A striking property of phosphorene nanoribbon is the presence of a quasi-flat edge band [24–27] that is entirely detached from the bulk band. We explore the band structure of phosphorene nanoribbon analytically and numerically as a continuous deformation of the honeycomb lattice by changing the transfer energy parameters t_i. The graphene is well explained in terms of electron hopping between the first neighbor sites with $t_1 = t_2 \neq 0$ and $t_3 = t_4 = t_5 = 0$, where the origin of the flat band has been argued to be topological [29]. We are able to employ the same argument to show the topological origin of the quasi-flat edge band in phosphorene. The essential roles are played by the ratio $|t_2/t_1|$ and t_4: The flat bands are detached from the bulk band when the ratio is 2, while the flat bands are bent due to the transfer energy t_4.

2. Model hamiltonian

The tight-binding model is given by

$$H_4 = \sum_{\langle i,j \rangle} t_{ij} c_i^\dagger c_j, \tag{1}$$

where summation runs over the lattice sites, t_{ij} is the transfer energy between ith and jth sites, and $c_i^\dagger$ (c_j) is the creation (annihilation) operator of electrons at site i (j). It has been shown [28] that it is enough to take five hopping links to describe phosphorene, as illustrated in figure 1. The transfer energy explicitly reads as $t_1 = -1.220\,\mathrm{eV}$, $t_2 = 3.665\,\mathrm{eV}$, $t_3 = -0.205\,\mathrm{eV}$, $t_4 = -0.105\,\mathrm{eV}$, $t_5 = -0.055\,\mathrm{eV}$ for these links.

2.1. Four-band tight-binding model

The unit cell of phosphorene contains four phosphorus atoms, where two phosphorus atoms exist in the upper layer and the other two phosphorus atoms exist in the lower layer. In the momentum representation we obtain the four-band Hamiltonian $H_4 = \sum_{\boldsymbol{k}} c^\dagger(\boldsymbol{k}) \hat{H}_4(\boldsymbol{k}) c(\boldsymbol{k})$ with

$$\hat{H}_4 = \begin{pmatrix} 0 & f_1 + f_3 & f_4 & f_2 + f_5 \\ f_1^* + f_3^* & 0 & f_2 & f_4 \\ f_4^* & f_2^* & 0 & f_1 + f_3 \\ f_2^* + f_5^* & f_4^* & f_1^* + f_3^* & 0 \end{pmatrix}, \tag{2}$$

where

$$f_1 = 2t_1 e^{i\frac{1}{2\sqrt{3}}a_x k_x} \cos\frac{1}{2}a_y k_y, \quad f_2 = t_2 e^{-i\frac{1}{\sqrt{3}}a_x k_x}, \quad f_3 = 2t_3 e^{-i\frac{5}{2\sqrt{3}}a_x k_x} \cos\frac{1}{2}a_y k_y,$$
$$f_4 = 4t_4 \cos\frac{\sqrt{3}}{2}a_x k_x \cos\frac{1}{2}a_y k_y, \quad f_5 = t_5 e^{2i\frac{1}{\sqrt{3}}a_x k_x}, \tag{3}$$

where a_x and a_y are the length of the unit cell into the x and y directions. We show the Brillouin zone and the energy spectrum of the tight-binding model in figures 2(a) and (c), respectively.

2.2. Two-band tight-binding model

We are able to reduce the four-band model to the two-band model due to the D_{2h} point group invariance. We focus on a blue point (atom in upper layer) and view other lattice points in the crystal structure (figure 1). We also focus on a red point (atom in lower layer) and view other lattice points. As far as the transfer energy is concerned, the two views are identical. Namely, we may ignore the color of each point. Hence, instead of the unit cell containing four points, it is enough to consider the unit cell containing only two points. This reduction makes our analytical study considerably simple.

The two-band model is given by $H_2 = \sum_{\boldsymbol{k}} c^\dagger(\boldsymbol{k}) \hat{H}_2(\boldsymbol{k}) c(\boldsymbol{k})$ with

$$\hat{H}_2 = \begin{pmatrix} f_4 & f_1 + f_2 + f_3 + f_5 \\ f_1^* + f_2^* + f_3^* + f_5^* & f_4 \end{pmatrix}. \tag{4}$$

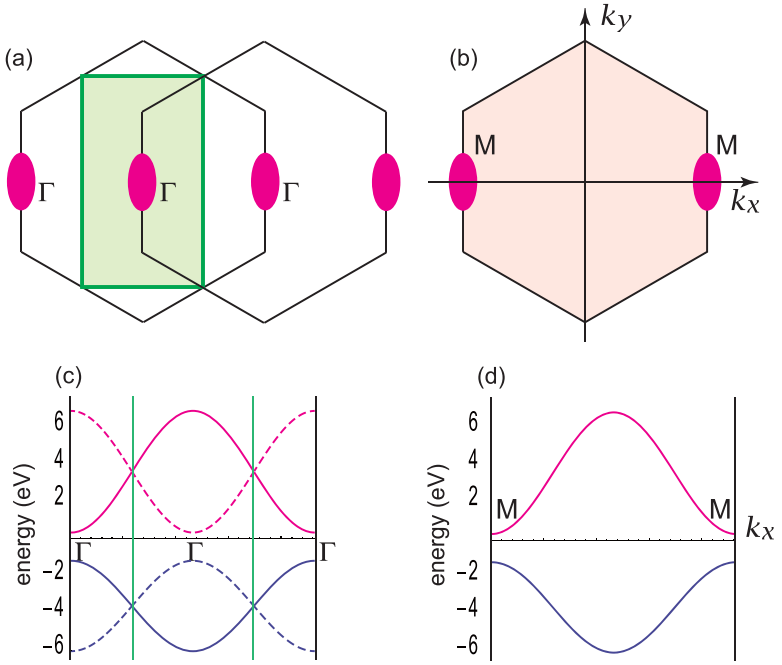

Figure 2. Brillouin zones and energy spectra of the four-band and two-band models of phosphorene. (a) The Brillouin zone is a rectangular in the four-band model, which is constructed from two copies of the hexagonal Brillouin zone of the two-band model. A magenta oval denotes a Dirac cone present at the Γ point. (b) The Brillouin zone is a hexagonal in the two-band model. A magenta oval denotes a Dirac cone present at the M point. (c) The band structure of the four-band model, which is constructed from two copies of that of the two-band model. (d) The band structure of the two-band model.

The rectangular Brillouin zone of the four-band model is constructed by folding the hexagonal Brillouin zone of the two-band model, as illustrated in figure 2(a).

The equivalence between the two models (2) and (4) is verified as follows. We have explicitly shown the energy spectra of the four-band model (2) and the two-band model (4) in figures 2(c) and (d), respectively. It is demonstrated that the energy spectrum of the four-band model is constructed from that of the two-band model: The two bands are precisely common between the two models, while the extra two bands in the four-band model are obtained simply by shifting the two bands of the two-band model, as dictated by the folding of the Brillouin zone.

By diagonalizing the Hamiltonian, the energy spectrum reads

$$E(\boldsymbol{k}) = f_4 \pm \left| f_1 + f_2 + f_3 + f_5 \right|. \tag{5}$$

The band gap is given by

$$\Delta = 4t_1 + 2t_2 + 4t_3 + 2t_5 = 1.52\,\mathrm{eV}. \tag{6}$$

The asymmetry between the positive and negative energies arises from the f_4 term.

2.3. Low-energy theory

In the vicinity of the Γ point, we make a Tayler expansion of f_i in (3) and obtain

$$\begin{aligned}
f_1 &= t_1\left(2 + \frac{i}{\sqrt{3}}a_xk_x - \frac{1}{12}\left(a_xk_x\right)^2 - \frac{1}{4}\left(a_yk_y\right)^2\right),\\
f_2 &= t_2\left(1 - \frac{i}{\sqrt{3}}a_xk_x - \frac{1}{6}\left(a_xk_x\right)^2\right),\\
f_3 &= t_3\left(2 - \frac{5i}{\sqrt{3}}a_xk_x - \frac{25}{12}\left(a_xk_x\right)^2 - \frac{1}{4}\left(a_yk_y\right)^2\right),\\
f_4 &= t_4\left(4 - \frac{3}{2}\left(a_xk_x\right)^2 - \frac{1}{2}\left(a_yk_y\right)^2\right),\\
f_5 &= t_5\left(1 + \frac{2i}{\sqrt{3}}a_xk_x - \frac{2}{3}\left(a_xk_x\right)^2\right).
\end{aligned} \tag{7}$$

The Hamiltonian (4) reads

$$\hat{H}_2 = f_4 + \left[\varepsilon + \alpha\left(a_xk_x\right)^2 + \beta\left(a_yk_y\right)^2\right]\tau_x + \gamma a_xk_x\tau_y, \tag{8}$$

with the Pauli matrices $\boldsymbol{\tau}$, where

$$\begin{aligned}
&m = 2t_1 + t_2 + 2t_3 + t_5 = 0.76\ \text{eV},\ \ \alpha = -\frac{1}{12}t_1 - \frac{1}{6}t_2 - \frac{25}{12}t_3 - \frac{3}{2}t_4 - \frac{2}{3}t_5 = 0.112\ \text{eV},\\
&\beta = -\frac{1}{4}t_1 + \frac{1}{4}t_3 + \frac{1}{2}t_4 = 0.201\ \text{eV},\ \ \gamma = \frac{1}{\sqrt{3}}\left(-t_1 + t_2 + 5t_3 - 2t_5\right) = 2.29\ \text{eV}.
\end{aligned} \tag{9}$$

Hence, the dispersion is linear in the k_y direction, but parabolic in the k_y direction. The energy spectrum is given by

$$E = f_4 \pm E_0, \tag{10}$$

with

$$E_0 = \sqrt{\gamma k_x^2 + \left[m + \alpha\left(a_xk_x\right)^2 + \beta\left(a_yk_y\right)^2\right]^2}. \tag{11}$$

The low-energy Hamiltonian agrees with the previous result [30] with a rotation of the Pauli matrices $\tau_x \mapsto \tau_z$ and $\tau_y \mapsto \tau_x$.

3. Phosphorene nanoribbons

We investigate the band structure of a phosphorene nanoribbon placed along the y direction (figure 1). There are two ways of cutting a honeycomb lattice along the y direction, yielding a zigzag edge and a beard edge. Accordingly, there are three types of nanoribbons, whose edges are (a) both zigzag, (b) zigzag and beard, (c) both beard. We show their band structures in figures 3(a), (b) and (c), respectively.

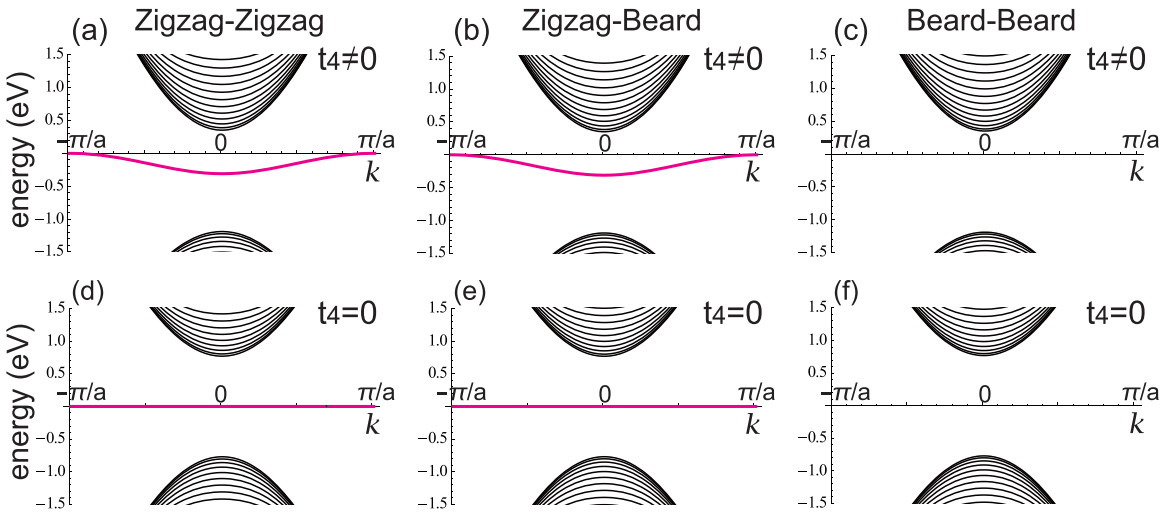

Figure 3. Band structure of phosphorene nanoribbons when the transfer energy t_4 is nonzero and zero. (a, d) Both edges are zigzag. (b, e) One edge is zigzag and the other edge is beard. (c, f) Both edges are beard. The quasi-flat edge mode emerges for (a) and (b). When we set $t_4 = 0$, the quasi-flat band becomes perfectly the flat band. Flat and quasi-flat edge states are marked in magenta.

3.1. Quasi-flat bands

A prominent feature of a phosphorene nanoribbon is the presence of the quasi-flat edge modes isolated from the bulk modes found in figures 3(a) and (b). They are doubly degenerate for a zigzag–zigzag nanoribbon, and nondegenerate for a zigzag-beard nanoribbon, while they are absent in a beard–beard nanoribbon [figure 3(c)].

We explore the mechanism of how such an isolated quasi-flat band emerges in phosphorene. As far as the energy spectrum is concerned, instead of $\hat{H}_2(k_x, k_y)$ as defined by (4), it is enough to analyze the two-band Hamiltonian

$$\hat{H}_2'\left(k_x, k_y\right) = \hat{H}_2\left(k_x, k_y\right) - f_4\left(k_x, k_y\right). \tag{12}$$

The term $f_4(k_x, k_y)$ only shifts the energy spectrum. The energy spectrum of $\hat{H}_2'(k_x, k_y)$ is symmetric between the positive and negative energy spectra, as we have noticed in (5). We show the band structures of the three types of nanoribbons in figures 3(d), (e) and (f) for the Hamiltonian $\hat{H}_2'(k_x, k_y)$, where the quasi-flat edge modes are found to become perfectly flat.

It is a good approximation to set $t_3 = t_5 = 0$, since the transfer energies t_1 and t_2 are much larger than the others. Indeed, we have checked numerically that almost no difference is induced by this approximation. The two-band model $\hat{H}_2'(k_x, k_y)$ is well approximated by the anisotropic honeycomb model,

$$\hat{H}_2'' = \begin{pmatrix} 0 & f_1 + f_2 \\ f_1^* + f_2^* & 0 \end{pmatrix}. \tag{13}$$

This Hamiltonian has been studied in the context of strained graphene and optical lattice [31–34]. The energy spectrum reads

$$E = \sqrt{t_2^2 + 4\left(t_1^2 + t_1 t_2 \cos\frac{\sqrt{3}}{2}a_x k_x\right)\cos\frac{1}{2}a_y k_y}, \tag{14}$$

which implies the existence of two Dirac cones at $k_x = 0$ and $k_y = k_{\rm D}$ with

$$ak_{\rm D} = 2\arctan\left(\sqrt{4t_1^2 - t_2^2}\big/t_2\right), \tag{15}$$

for $|t_2| < 2|t_1|$, where we have set $a = a_y$.

3.2. Flat bands in anisotropic honeycomb lattice

We explore the origin of the flat band in the anisotropic honeycomb-lattice model (13). It is instructive to study the change of the band structure of nanoribbon by changing the parameter t_2 continuously, with t_1 being fixed. We show the band structure with (a) the zigzag–zigzag edges, (b) the zigzag-beard edges, and (c) the beard–beard edges in figure 4 for typical values of t_1 and t_2.

(i) We start with the case $t_2 = |t_1|$, where the energy spectrum (14) becomes that of graphene with two Dirac cones at the K and K' points. The perfect flat band connects the K and K' points, that is, it lies for (a) $-\pi \leqslant ak \leqslant -\frac{2}{3}\pi$ and $\frac{2}{3}\pi \leqslant ak \leqslant \pi$; (b) $-\pi \leqslant ak \leqslant \pi$; (c) $-\frac{2}{3}\pi \leqslant ak \leqslant \frac{2}{3}\pi$. It is attached to the bulk band. See figures 4(a)–(c).

(ii) As we increase t_2 but keep t_1 fixed, the two Dirac points move towards $k = 0$, as is clear from (15). The flat band is kept be present and connects the two Dirac points. See figures 4 (d)–(f).

(iii) At $|t_2| = 2|t_1|$, the two Dirac points merge into one Dirac point at $k = 0$, as implied by (15). The flat band touches the bulk band at $k = 0$ for the zigzag–zigzag nanoribbon and the zigzag-beard nanoribbon, but disappears from the beard–beard nanoribbon. See figures 4(g)–(i).

(iv) For $|t_2| > 2|t_1|$, the bulk band shifts away from the Fermi level, as follows from (14). The flat band is disconnected from the bulk band for the zigzag–zigzag nanoribbon and the zigzag-beard nanoribbon, where it extends over all of the region $-\pi \leqslant k \leqslant \pi$. On the other hand, the edge band becomes a part of the bulk band and disappears from the Fermi level for the beard–beard nanoribbon. See figures 4(j)–(l).

3.3. Topological origin of flat bands

The topological origin of the flat band has been discussed in graphene [29]. It is straightforward to apply the reasoning to the anisotropic honeycomb-lattice model (13). We consider one-dimensional (1D) Hamiltonian $H_k(k_x)$ in the k_x space, which is essentially given by the two-band model (13) at a fixed value of $k \equiv k_y$. We analyze the topological property of this 1D Hamiltonian. Because the k_x space is a circle due to the periodic condition, the homotopy class is $\pi_1(S^1) = \mathbb{Z}$.

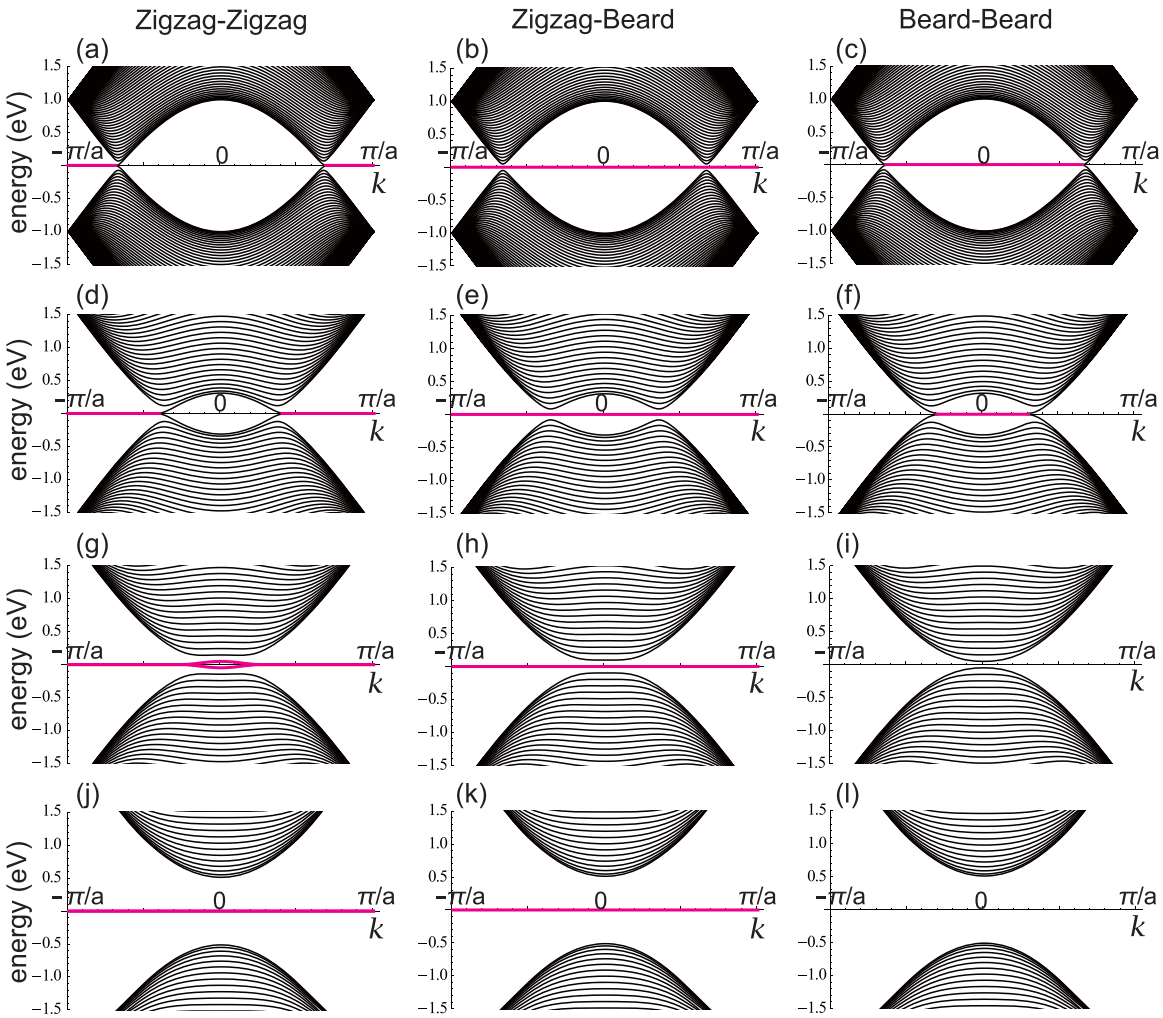

Figure 4. Band structure of anisotropic honeycomb nanoribbons. The flat edge states are marked in magenta. We have set $t_1 = -1$ and $t_3 = t_4 = t_5 = 0$. We have also set (a, b, c) $t_2 = 1$, (d, e, f) $t_2 = 1.7$, (g, h, i) $t_2 = 2$, (j, k, l) $t_2 = 2.5$. The unit cell contains 144 atoms.

We write the Hamiltonian as

$$H_k(k_x) = \begin{pmatrix} 0 & F_k(k_x) \\ F_k^*(k_x) & 0 \end{pmatrix}. \tag{16}$$

It is important to remark that the gauge degree of freedom is present in this Hamiltonian [35]. Indeed the phase of the term $F_k(k_x)$ is irrelevant for the energy spectrum of the bulk system. However, this is not the case for the analysis of a nanoribbon, since the way of taking the unit cell is inherent to the type of nanoribbon, as illustrated in figure 5. It is necessary to make a gauge fixing so that the hopping between the two atoms in the unit cell becomes real, namely, t_1 for the zigzag edge and t_2 for the beard edge.

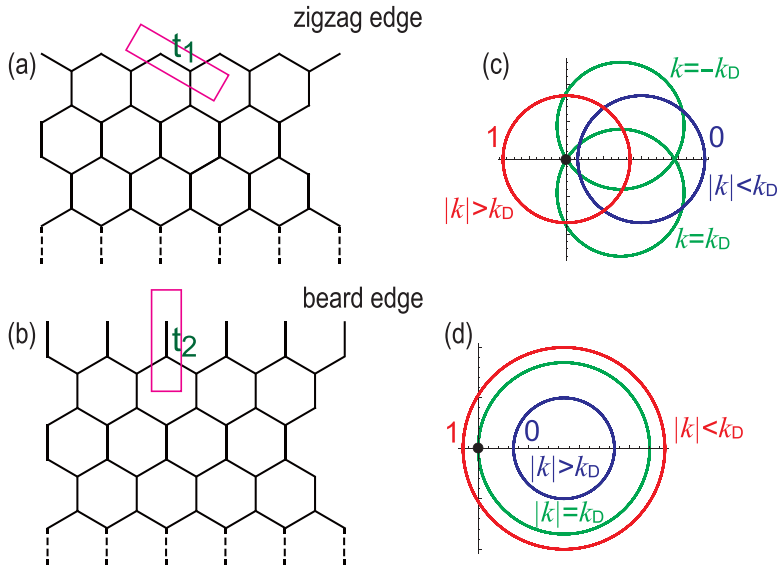

Figure 5. Unit cells and winding numbers for the zigzag and beard edges. It is necessary to make a gauge fixing in the Hamiltonian so that the hopping between the two atoms in the unit cell becomes real, namely, (a) t_1 for the zigzag edge and (b) t_2 for the beard edge. (c, d) The winding number reads $N_{\rm wind}(k) = 1$ if the loop encircles the origin (red circle), and $N_{\rm wind}(k) = 0$ if not (blue circle). The origin is represented by a dot, where the Hamiltonian is ill defined.

For the zigzag edge we thus make the gauge fixing such that

$$F_k(k_x) = e^{-i\left(\frac{1}{2\sqrt{3}}a_x k_x + \frac{1}{2}ak\right)}\left(f_1 + f_2\right) = t_1\left(1 + e^{-iak}\right) + t_2 e^{-i\frac{1}{2}(\sqrt{3}a_x k_x - ak)},$$

where the parameter k corresponds to the momentum of zigzag nanoribbons. Here, t_1 for the link in the unit cell and $e^{-iak}t_1$ for the neighboring link [figure 5(a)]. The topological number of the 1D system is given by

$$N_{\rm wind}(k) = \int_{-\pi/a}^{\pi/a} dk_x\ \partial_{k_x} \log F_k(k_x). \tag{17}$$

By an explicit evaluation, $N_{\rm wind}(k)$ is found to take only two values; $N_{\rm wind} = 1$ for $|k| < k_{\rm D}$, and $N_{\rm wind} = 0$ for $\pi \geqslant |k| > k_{\rm D}$. We may interpret this as the winding number as follows. We consider the complex plane for $F_k(k_x) = |F_k(k_x)| \exp\left[i\Theta_k(k_x)\right]$. The quantity $N_{\rm wind}(k)$ counts how many times the complex number $F_k(k_x)$ winds around the origin as k_x moves from 0 to $2\pi/a$ for a fixed value of k. Note that the origin implies $F_k(k_x) = 0$, where the Hamiltonian is ill defined. We have shown such a loop for typical values of k in figure 5(b), where the horizontal axis is for Re $[F_k(k_x)]$ and the vertical axis is for Im $[F_k(k_x)]$,

$$\mathrm{Re}\left[F_k(k_x)\right] = t_1(1 + \cos ak) + t_2 \cos\frac{1}{2}\left(\sqrt{3}a_x k_x - ak\right), \tag{18a}$$

$$\mathrm{Im}\left[F_k(k_x)\right] = t_1 \sin ak + t_2 \sin\frac{1}{2}\left(\sqrt{3}a_x k_x - ak\right). \tag{18b}$$

The loop surrounds the origin and $N_{\rm wind}(k) = 1$ when $-\pi \leqslant k < -k_{\rm D}$ and $k_{\rm D} < k \leqslant \pi$, while it does not and $N_{\rm wind}(k) = 0$ when $|k| < k_{\rm D}$: The loop touches the origin when $k = \pm k_{\rm D}$. We have demonstrated that the system is topological for $|k| > k_{\rm D}$ and trivial for $|k| < k_{\rm D}$.

We next appeal to the bulk-edge correspondence to the topological system. When we cut the bulk along the y direction, the 1D system has an edge. Since the edge separates a topological insulator and the trivial state (i.e., the vacuum state), the gap must close at the edge, namely, there must appear a gapless edge mode. The gapless edge mode appears for all $|k| < k_{\rm D}$, implying the emergence of a flat band connecting the two Dirac points given by (15).

For the beard edge, we make the gauge fixing such that

$$F_k\left(k_x\right) = e^{i\frac{1}{\sqrt{3}}a_x k_x}\left(f_1 + f_2\right) \tag{19}$$

and carry out an analogous argument (see figure 5). We reach at the conclusion that a flat band appears for $|k| > k_{\rm D}$ and connects the two Dirac points given by (15) but in an opposite way to the case of the zigzag edge.

3.4. Wave function and energy spectrum of edge states

We have explained how the flat band appears in the anisotropic honeycomb-lattice model. The flat band corresponds to the quasi-flat band in the original Hamiltonian $\hat{H}_2$.

We construct an analytic form of the wave function at the zero-energy state in the anisotropic honeycomb-lattice model (13) as follows. We label the wave function of the atom on the outer most cite as ψ_1, and that of the atom next to it as ψ_2, and as so on. The total wave function is $\psi = \left\{\psi_1, \psi_2, \cdots, \psi_N\right\}$ if there are N atoms across the nanoribbon. The Hamiltonian is explicitly written as

$$H = \begin{pmatrix} 0 & t_1 g & 0 & 0 & \cdots \\ t_1 g^* & 0 & t_2 & 0 & \cdots \\ 0 & t_2 & 0 & t_1 g & \cdots \\ 0 & 0 & t_1 g^* & 0 & \cdots \\ \cdots & \cdots & \cdots & \cdots & \cdots \end{pmatrix}, \tag{20}$$

with $g = 1 + e^{-iak}$. The eigenvalue problem $H\psi = 0$ is easily solved [36], yielding $\psi_{2n} = 0$ and $\psi_{2n+1} = [t_1(1 + e^{iak})/t_2]^n \psi_1$. By solving the Hamiltonian matrix recursively from the outer most cite, we obtain the analytic form of the local density of states of the wave function for odd cite j,

$$|\psi(j)| = \alpha^j \sqrt{1 - \alpha^2}, \tag{21}$$

with $\alpha = 2|t_1|(\cos\frac{ak}{2})\big/|t_2|$. The wave function is zero for even cite. It is perfectly localized at the outermost site when $ak = \pi$, and describes the flat band.

We can derive the energy spectrum of the quasi-flat band perturbatively. With the use of this wave function, the energy spectrum $E_{\rm qf}(k)$ of the quasi-flat band is estimated perturbatively by taking the expectation value of the t_4 term as

$$E_{\rm qf}(k) = \sum_{n=0}^{\infty} t_4\left(1 + e^{-iak}\right)\psi_n^* \psi_{n+2} + t_4\left(1 + e^{iak}\right)\left(\psi_{n+2}^* \psi_n\right) = -\frac{4t_1 t_4}{t_2}(1 + \cos ak), \tag{22}$$

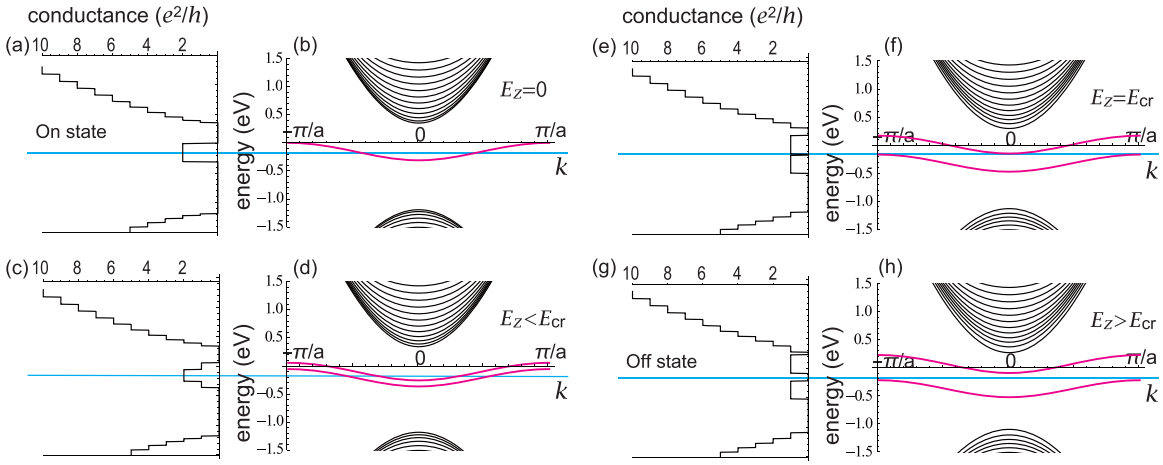

Figure 6. Band structure and conductance in unit of e^2/h of phosphorene nanoribbons with the both edges being zigzag in the presence of in-plane electric field E_x. (a, b) $E_x = 0$, (c, d) $E_x = 0.5\,\mathrm{meV/nm}$, (e, f) $E_x = 1.5\,\mathrm{meV/nm}$, (g, h) $E_x = 2.0\,\mathrm{meV/nm}$. Magenta curves represent the quasi-flat bands, while cyan lines represent the Fermi energy. The unit cell contains 144 atoms.

where $4t_1t_4/t_2 = 0.14$. On the other hand, we numerically obtain $E(0) = -0.301\,\mathrm{eV}$. The agreement is excellent.

4. Nanoribbons with in-plane electric field

It is possible to make a significant change of the quasi-flat edge band by applying external electric field parallel to the phosphorene sheet as in the case of graphene nanoribbon [4]. Let us apply electric field E_x into the x direction of a nanoribbon with zigzag–zigzag edges. A large potential difference ($\propto WE_x$) is possible between the two edges if the width W of the nanoribbon is large enough. This potential difference resolves the degeneracy of the two edge modes, shifting one edge mode upwardly and the other downwardly without changing their shapes. We present the resultant band structures in figure 6 for typical values of E_x.

The energy shift due to the in-plane electric field is given by

$$\Delta E(k) = \sum_{n=0}^{\infty} (W - n) \left|\psi_n\right|^2 = \left(W - \frac{\alpha^2}{1-\alpha^2} \right) E_x. \tag{23}$$

This is well approximated by $\Delta E(k) = WE_x$ for wide nanoribbons.

Electric current may flow along the edge. We derive the conductance. In terms of single-particle Green's functions, the low-bias conductance $\sigma(E)$ at the Fermi energy E is given by [37]

$$\sigma(E) = \left(e^2/h\right) \mathrm{Tr}\left[\Gamma_{\mathrm{L}}(E) G_{\mathrm{D}}^{\dagger}(E) \Gamma_{\mathrm{R}}(E) G_{\mathrm{D}}(E) \right], \tag{24}$$

where $\Gamma_{\mathrm{R(L)}}(E) = i\left[\Sigma_{\mathrm{R(L)}}(E) - \Sigma_{\mathrm{R(L)}}^{\dagger}(E)\right]$ with the self-energies $\Sigma_{\mathrm{L}}(E)$ and $\Sigma_{\mathrm{R}}(E)$, and

$$G_{\mathrm{D}}(E) = \left[E - H_{\mathrm{D}} - \Sigma_{\mathrm{L}}(E) - \Sigma_{\mathrm{R}}(E) \right]^{-1}, \tag{25}$$

with the Hamiltonian $H_{\rm D}$ for the device region. The self-energy $\Sigma_{\rm L(R)}(E)$ describes the effect of the electrode on the electronic structure of the device, whose the real part results in a shift of the device levels, whereas the imaginary part provides a life time. It is to be calculated numerically [38–41].

We use this formula to derive the conductance,

$$\frac{e^2}{h}\Big[\theta\big(E-\varepsilon_0-|\Delta E(0)|\big)-\theta(E-|\Delta E(\pi)|)+\theta\big(E-\varepsilon_0+|\Delta E(0)|\big)-\theta(E+|\Delta E(\pi)|)\Big],$$

where $\theta(x)$ is the step function $\theta=1$ for $x>0$ and $\theta=0$ for $x<0$. We show the conductance in figure 6. Without in-plane electric field, the conductance at the Fermi energy is $2e^2/h$ since there is a two-fold degenerate quasi-flat band. Above the critical electric field, the conductance becomes 0 since the quasi-flat band splits perfectly. The critical electric field is determined as

$$E_{\rm cr}=\big|\varepsilon_0\big|/(2W) \tag{26}$$

The critical electric field is anti-proportional to the width W. This acts as a field-effect transistor driven by in-plane electric field.

5. Conclusion

We have analyzed the band structure of phosphorene nanoribbons based on the tight-binding model, and demonstrated the presence of quasi-flat edge modes entirely detached from the bulk band. We have shown the topological origin of the flat band in the anisotropic honeycomb-lattice (13) or, equivalently m the quasi-flat band in the original two-band model (4). The flat band bends because it is simply sifted by the transfer energy ($\propto t_4$) dependent of the momentum k and becomes a quasi-flat band. The energy spectrum is given by (22) in the lowest order of perturbation.

Acknowledgements

The author is very much grateful to N. Nagaosa and A.-L. Phaneuf-l'heureux for many helpful discussions on the subject. He thanks the support by the Grants-in-Aid for Scientific Research from the Ministry of Education, Science, Sports and Culture No. 25400317.

References

[1] Castro Neto A H, Guinea F, Peres N M R, Novoselov K S and Geim A K 2009 *Rev. Mod. Phys.* **81** 109
[2] Katsnelson M I 2012 *Graphene: Carbon in Two Dimensions* (Cambridge: Cambridge University Press)
[3] Fujita M *et al* 1996 Peculiar Localized State at Zigzag Graphite Edge *J. Phys. Soc. Japan* **65** 1920
[4] Son Y-W, Cohen M L and Louie S G 2006 *Nature* **444** 347
[5] Ezawa M 2006 *Phys. Rev.* B **73** 045432
[6] McCann E and Fal'ko V I 2006 *Phys. Rev. Lett.* **96** 086805
[7] Liu C-C, Feng W and Yao Y 2011 *Phys. Rev. Lett.* **107** 076802
[8] Vogt P, de Padova P, Quaresima C, Frantzeskakis E, Asensio M C, Resta A, Ealet B and Lay G L 2012 *Phys. Rev. Lett.* **108** 155501
[9] Fleurence A, Friedlein R, Ozaki T, Kawai H, Wang Y and Yamada-Takamura Y 2012 Experimental Evidence for Epitaxial Silicene on Diboride Thin Films *Phys. Rev. Lett.* **108** 245501

[10] Lin C-L, Arafune R, Kawahara K, Tsukahara N, Minamitani E, Kim Y, Takagi N and Kawai M 2012 *Appl. Phys. Expr.* **5** 045802
[11] Mak K F, Lee C, Hone J, Shan J and Heinz T F 2010 *Phys. Rev. Lett.* **105** 136805
[12] Zeng H, Dai J, Yao W, Xiao D and Cui X 2012 *Nature Nanotech.* **7** 490
[13] Cao T *et al* 2012 *Nat. Com.* **3** 887
[14] Li L, Yu Y, Ye G J, Ge Q, Ou X, Wu H, Feng D, Chen X H and Zhang Y 2014 *Nature Nanotech.* **9** 372
[15] Liu H, Neal A T, Zhu Z, Xu X, Tomanek D and Ye P D 2014 *ACS Nano* **8** 4033
[16] Xia F, Wang H and Jia Y 2014 *Nature Commun.* **5** 4458
[17] Castellanos-Gomez A *et al* 2014 *2D Mat.* **1** 025001
[18] Koenig S P, Doganov R A, Schmidt H, Castro Neto A H and Oezyilmaz B 2014 *Appl. Phys. Lett.* **104** 103106
[19] Peng X, Copple A and Wei Q 2014 *Phys. Rev.* B **90** 085402
[20] Tran V, Soklaski R, Liang Y and Yang L 2014 *Phys. Rev.* B **89** 235319
[21] Qiao J, Kong X, Hu Z-X, Yang F and Ji W 2014 *Nature Commun.* **5** 4475
[22] Fei R and Yang L 2014 *Nano Lett.* **14** 2884
[23] Tran V and Yang L 2014 *Phys. Rev.* B **89** 245407
[24] Guo H, Lu N, Dai J, Wu X and Zeng X C 2014 *J. Phys. Chem.* C **118** 14051
[25] Maity A, Singh A and Sen P 2014 arXiv:1404.2469
[26] Carvalho A, Rodin A S and Castro Neto A H 2014 arXiv:1404.5115
[27] Peng X, Wei Q and Copple A 2014 *J. Appl. Phys.* **116** 144301
[28] Rudenko N and Katsnelson M I 2014 *Phys. Rev.* B **89** 201408
[29] Shinsei R and Hatsugai Y 2002 *Phys. Rev. Lett.* **89** 077002
[30] Rodin A S, Carvalho A and Castro Neto A H 2014 *Phys. Rev. Lett.* **112** 176801
[31] Pereira V M, Castro Neto A H and Peres N M R 2009 *Phys. Rev.* B **80** 045401
[32] Montambaux G, Piéchon F, Fuchs J-N and Goerbig M O 2009 *Phys. Rev.* B **80** 153412
[33] Wunsch B, Guinea F and Sols F 2008 *New. J. Phys.* **10** 103027
[34] Tarruell L *et al* 2012 *Nature* **483** 7389
[35] Kariyado T and Hatsugai Y 2013 *Phys. Rev.* B **88** 245126
[36] Kohmoto M and Hasegawa Y 2007 *Phys. Rev.* B **76** 205402
[37] Datta S 1995 *Electronic Transport in Mesoscopic Systems* (Cambridge: Cambridge University Press)
Datta S 2005 *Quantum Transport: Atom to Transistor* (Cambridge: Cambridge University Press)
[38] Sancho M P, Sancho J M L and Rubio J 1985 *J. Phys. F: Met. Phys* **15** 851
[39] Muñoz-Rojas F, Jacob D, Fernández-Rossier J and Palacios J J 2006 *Phys. Rev.* B **74** 195417
[40] Zârbo L P and Nikolić B K 2007 *EPL* **80** 47001
Areshkin D A and Nikolić B K 2009 *Phys. Rev.* B **79** 205430
[41] Ezawa M 2013 *Appl. Phys. Lett.* **102** 172103